Available on: http://gjetr.ep-journals.org/ E-ISSN: 3051-3782, P-ISSN: 3051-3774

Global Journal of Engineering and Technology Review

Volume: 02 Issue: 01 January 2026

Field-Oriented Speed Control of Three-Phase Induction Motors Considering Iron Losses in the Magnetizing Branch

Duy Khuong Nguyen
Equipment Management Department, Ton Duc Thang University, Ho Chi Minh City, Vietnam

Thinh Ba Cong Huynh
Faculty of Electrical and Electronics Engineering, Ton Duc Thang University, Ho Chi Minh City, Vietnam

Published Date: January 23, 2026 **Article DOI: 10.65150/EP-gjetr/V2E1/2026-03**

ABSTRACT: Field-Oriented Control (FOC) has long established its superiority in controlling three-phase induction motors due to its ability to decouple torque and flux control. However, conventional FOC models typically rely on the idealized assumption of neglecting iron losses in the magnetizing branch. This leads to significant inaccuracies in estimating rotor flux amplitude and position, particularly during high-speed operation or under large slip frequency variations. This study focuses on a speed-controlled FOC solution that explicitly accounts for iron-loss components by integrating an equivalent iron-loss resistance into the mathematical model within the stationary reference frame. Simulation results demonstrate that by incorporating iron losses into the control architecture, the error between actual and reference speeds is minimized, the electromagnetic torque response becomes more precise relative to the load, and the system's energy efficiency is markedly improved compared to traditional FOC methods. This research provides a robust solution to enhance the reliability and precision of high-performance industrial electric drive systems.

KEYWORDS: Field-Oriented Control, Induction Motor, Iron Loss, Current Model, Energy Efficiency, Speed Control.

INTRODUCTION

Three-phase induction motors are the dominant consumers of electricity in industrial sectors. Therefore, optimizing their efficiency and dynamic performance is a critical goal from both economic and environmental standpoints (Abdin et al., 2003). Beyond pure efficiency, modern control systems also demand high reliability and robustness, requiring continuous operation even in the face of parameter variations or sensor faults (Tran et al., 2024; Tran et al., 2025a).

Field-Oriented Control (FOC) has become the industry standard because it effectively decouples torque and flux components, allowing for precise speed regulation comparable to DC motors (Abu-Rub et al., 2021; Rivera et al., n.d.). However, a major limitation of conventional FOC schemes is their reliance on simplified mathematical models that ignore iron losses to save computational power. Research indicates that while iron losses may only account for 1–4% of rated power, they are a critical factor for model accuracy (Bašić & Vukadinović, 2018; Levi, 1995; Rivera et al., n.d.). Ignoring this component distorts the estimation of rotor flux and electromagnetic torque, while also causing deviations in the rotor time constant.

These inaccuracies can severely compromise the stability of vector control algorithms. This is particularly evident during light-load operation or variable-speed conditions, where the ratio of iron losses to copper losses shifts, leading to significant efficiency drops (Abdin et al., 2003; Ayana et al., 2023; Levi, 1995). Fortunately, the advent of high-speed digital signal processors has made it feasible to implement higher-order models that explicitly account for these losses. Specifically, integrating an iron-loss resistance into the magnetizing branch creates a sixth-order dynamic model that mirrors the machine's actual electromagnetic behavior much more closely (Abu-Rub et al., 2021; Dittrich, 1998; Rivera et al., n.d.). This refinement is essential for correcting flux orientation and mitigating errors caused by iron-loss currents.

To address this gap, this study investigates an indirect rotor flux-oriented speed control strategy that explicitly incorporates iron losses within the magnetizing branch. We developed and evaluated a high-order mathematical model using MATLAB/Simulink. The proposed approach is designed to enhance dynamic stability and control precision while simultaneously boosting energy efficiency. Through comparative simulations between an ideal model and our iron-loss-inclusive model, this paper demonstrates the practical necessity of accounting for iron losses in high-performance induction motor drive systems (Bašić et al., 2023; Rivera et al., n.d.).

LITERATURE REVIEW

Field-oriented control (FOC) has been extensively investigated and widely adopted in high-performance induction motor drive systems due to its capability to decouple torque and flux dynamics. Since its introduction, various FOC schemes have been developed, including direct rotor flux-oriented control (RFOC) and indirect rotor flux-oriented control (IRFOC). Among these approaches, IRFOC is particularly attractive for industrial applications owing to its relatively simple structure and reduced reliance on direct flux sensing, while still providing satisfactory dynamic performance under nominal operating conditions (Rivera et al., n.d.).

Most conventional FOC-based control strategies rely on simplified mathematical models of induction motors, in which magnetic saturation and iron losses are typically neglected to reduce model order and computational burden. Under these assumptions, the magnetizing branch is often represented by a pure inductance, implying that all magnetizing current contributes directly to flux production. Although this approximation is acceptable under rated operating conditions, its accuracy deteriorates significantly during light-load operation and variable-speed regimes (Abdin et al., 2003; Abu-Rub et al., 2021; Levi, 1995).

Numerous studies have demonstrated that iron losses, commonly modeled by an equivalent resistance connected in parallel with the magnetizing inductance, exert a non-negligible influence on the electromagnetic behavior of induction motors. Research findings indicate that although these losses constitute a minor percentage of the machine's total power rating, they introduce parasitic current components that do not contribute to torque production (Abu-Rub et al., 2021; Bašić & Vukadinović, 2018; Dittrich, 1998; Levi, 1995). Neglecting these losses results in inaccuracies in rotor flux estimation, electromagnetic torque calculation, and rotor time constant identification. Consequently, the performance of flux-oriented control schemes may be adversely affected, leading to flux detuning, reduced efficiency, and degraded dynamic response (Ayana et al., 2023; Levi, 1995).

To address these issues, various iron-loss modeling approaches have been proposed in the literature, including frequency-dependent loss models, nonlinear iron-loss representations, and equivalent iron-loss resistance models incorporated into the magnetizing branch. Among these methods, the equivalent iron-loss resistance approach has gained considerable attention due to its simplicity and compatibility with analytical modeling and control-oriented frameworks (Abu-Rub et al., 2021; Dittrich, 1998; Rivera et al., n.d.). However, a substantial portion of prior research has emphasized steady-state efficiency evaluation and loss minimization, while providing limited integration of iron-loss-aware models into the full closed-loop dynamic structure of FOC/IRFOC drives (Abdin et al., 2003; Dominguez et al., 2011).

More recent research efforts have investigated the impact of non-idealities and parameter variations on vector control performance using advanced control and observer-based strategies. Studies that explicitly incorporate iron-loss resistance into sensorless observer designs and predictive control frameworks have reported improved flux estimation accuracy, torque control, and efficiency across wider operating ranges (Ayana et al., 2023; Bašić & Vukadinović, 2018; Bašić et al., 2023). Beyond iron losses, recent works have also addressed the sensitivity of FOC to other parameter uncertainties and component failures. For instance, Tran et al. (2025a) proposed an MRAS-based approach to estimate stator resistance in real-time, thereby mitigating the impact of temperature variations on rotor flux angle estimation in sensorless control. Furthermore, to enhance system reliability, advanced fault-tolerant control strategies and sensor fault diagnosis methods based on rotor flux observers have been developed to maintain high performance even under sensor failure conditions (Tran et al., 2024; Tran et al., 2025b).

Nevertheless, many of these works focus on specific controller/observer implementations (e.g., predictive, sensorless, or fault-tolerant structures) and do not comprehensively examine the dynamic implications of iron-loss inclusion within an IRFOC-based speed control framework using a high-order induction motor model. Based on the above discussion, a clear research gap exists in the integration of iron-loss modeling within IRFOC frameworks using high-order induction motor models that simultaneously address flux orientation accuracy, dynamic stability, and energy efficiency. This observation motivates the present study, which develops a sixth-order dynamic model incorporating iron-loss resistance in the magnetizing branch and applies it to an IRFOC-based speed control scheme. Comparative simulation studies are conducted to demonstrate the necessity and effectiveness of accounting for iron losses in achieving accurate, stable, and energy-efficient induction motor drive performance.

MATERIALS AND METHODS

1. Materials

The study investigates a three-phase squirrel-cage induction motor, specifically the Siemens model 1LA7106-4AA10. The motor's rated parameters and electrical characteristics are derived from the manufacturer's technical documentation, serving as the foundation for modeling and analysis.

All simulations and evaluations are conducted within the MATLAB/Simulink environment. This platform enables the implementation and comparison of two models: an ideal induction motor model and a modified T-equivalent circuit model, in which iron losses are represented by an equivalent iron-loss resistance in the magnetizing branch (Abu-Rub et al., 2021, Chapter 5; Dittrich, 1998). This setup facilitates a quantitative analysis of the impact of iron losses on the dynamic behavior and efficiency of the drive system.

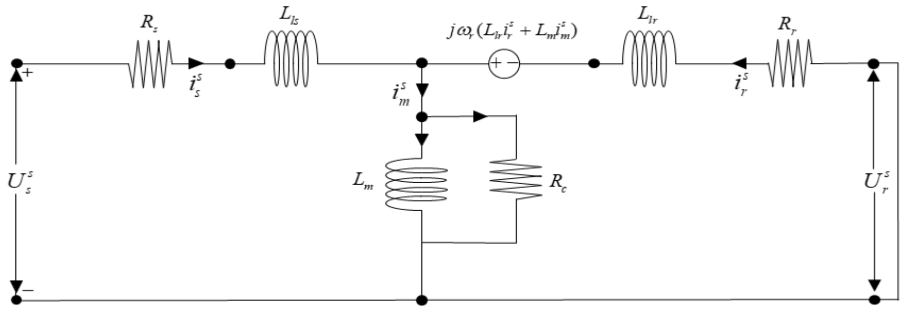

Figure 1: T-equivalent circuit of a three-phase induction motor in the αβ reference frame

2. METHODS

In this study, the electrical quantities of the three-phase induction motor are initially expressed in the stationary three-phase a-b-c reference frame. To facilitate vector-based analysis and control design, the Clarke transformation is applied to map these three-phase variables into the stationary two-axis α-β reference frame. This transformation reduces the number of variables required for dynamic modeling while preserving the machine's essential electromagnetic information (Abu-Rub et al., 2021, Chapter 5).

Based on the stationary α-β reference frame, the voltage, current, and flux equations are derived, forming the foundation for the high-order dynamic model and the Indirect Rotor Flux-Oriented Control (IRFOC) strategy (Rivera et al., n.d.).

The Clarke transformation used to convert the three-phase stator currents is given by:

$$\begin{bmatrix} i_{\alpha s} \\ i_{\beta s} \end{bmatrix} = \frac{2}{3}\begin{bmatrix} 1 & -\frac{1}{2} & -\frac{1}{2} \\ 0 & \frac{\sqrt{3}}{2} & -\frac{\sqrt{3}}{2} \end{bmatrix}\begin{bmatrix} i_{sa} \\ i_{sb} \\ i_{sc} \end{bmatrix} \tag{1}$$

In addition to the dynamic model in the stationary frame, the control structure employs the Park transformation to map motor variables into the rotating d-q reference frame. This step is critical for IRFOC as it facilitates indirect rotor flux orientation and enables independent control of electromagnetic torque and magnetizing current (Abu-Rub et al., 2021, Chapter 5).

The Park transformation is expressed as:

$$\begin{bmatrix} i_{ds} \\ i_{qs} \end{bmatrix} = \begin{bmatrix} \cos\theta_s & \sin\theta_s \\ -\sin\theta_s & \cos\theta_s \end{bmatrix}\begin{bmatrix} i_{\alpha s} \\ i_{\beta s} \end{bmatrix} \tag{2}$$

Using the T-equivalent circuit of the induction motor in the stationary α-β frame, which explicitly incorporates iron-loss resistance, the stator and rotor voltage equations, along with the flux linkage equations, are derived as follows:

$$\begin{cases} u_s^s = R_s i_s^s + \dfrac{d\psi_s^s}{dt} \\ 0 = R_r i_r^s + \dfrac{d\psi_r^s}{dt} - j\omega_r \psi_r^s \\ \psi_s^s = L_{ls} i_s^s + L_m i_m^s \\ \psi_r^s = L_{lr} i_r^s + L_m i_m^s \end{cases} \tag{3}$$

Starting from these four fundamental equations, appropriate variable transformations are applied to construct the state-space model. This results in a set of six dynamic equations (in real-signal form) that simulate the induction motor in the stationary α-β frame, involving the stator current $i_s{}^s$, magnetizing current $i_m{}^s$, and rotor flux $\psi_r{}^s$:

$$\begin{cases} \dfrac{di_s^s}{dt} = \left[\dfrac{1}{L_s - L_m}\right] u_s^s - \left[\dfrac{R_s + R_c}{L_s - L_m}\right] i_s^s - \left[\dfrac{R_c}{(L_r - L_m)(L_s - L_m)}\right]\psi_r^s + \left[\dfrac{R_c L_r}{(L_r - L_m)(L_s - L_m)}\right] i_m^s \\ \dfrac{di_m^s}{dt} = \left[\dfrac{R_c}{L_m}\right] i_s^s + \left[\dfrac{R_c}{L_m L_r - L_m{}^2}\right]\psi_r^s - \left[\dfrac{R_c L_r}{L_m L_r - L_m{}^2}\right] i_m^s \\ \dfrac{d\psi_r^s}{dt} = -\left[\dfrac{R_r}{L_r - L_m}\right]\psi_r^s + \left[\dfrac{R_r L_m}{L_r - L_m}\right] i_m^s + j\omega_r \psi_r^s \end{cases} \tag{4}$$

However, during operation, the iron-loss resistance R_c does not remain constant at its rated value. Instead, it varies significantly with operating conditions. The instantaneous value of R_c is determined by scaling its nominal value (obtained from no-load tests) based on changes in magnetic flux magnitude and supply frequency. Consequently, iron-loss resistance is modeled as a function of these two variables, as shown in Equation (5) (Bašić & Vukadinović, 2018; Dittrich, 1998; Levi, 1995):

$$R_c = R_{c-rated}\left(\frac{f_s}{f_{s-rated}}\right)^{1,1}\left(\frac{\psi_s}{\psi_{s-rated}}\right)^2 \tag{5}$$

Based on the mathematical model defined in Equation (4) and the variable resistance model in Equation (5), the three-phase induction motor is simulated in the stationary α-β reference frame using MATLAB/Simulink.

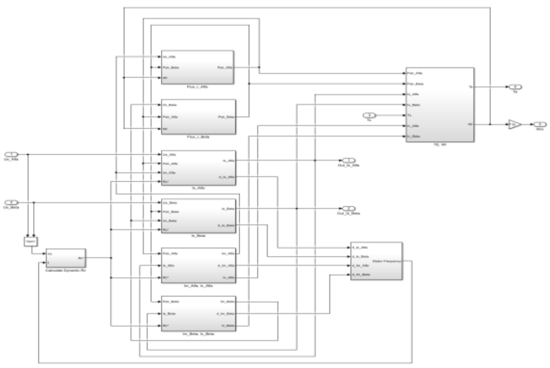

Figure 2: Three-Phase Induction Motors Considering Iron Losses in the Magnetizing Branch in MATLAB/Simulink

Corresponding Author: Thinh Ba Cong Huynh

Following the successful establishment of the three-phase induction motor's dynamic model, the subsequent phase of this research involves the development of a current-controlled Indirect Rotor Field Oriented Control (IRFOC) scheme. The primary objective of this control architecture is to achieve a complete decoupling between the electromagnetic torque and the rotor flux, effectively transforming the complex AC motor dynamics into a simplified structure analogous to a separately excited DC motor (Levi, 1995).

Within this framework, the stator current is decomposed into two orthogonal components in the synchronous d-q reference frame: the d-axis current i_{ds}, responsible for flux excitation, and the q-axis current i_{qs}, which directly regulates the torque. Unlike direct methods, the indirect approach utilizes the slip frequency relationship-derived from the motor parameters and current commands-to estimate the instantaneous position of the rotor flux without the need for direct flux sensors. Furthermore, by integrating the previously defined variable iron-loss resistance R_c into the IRFOC algorithm, the controller can compensate for parasitic currents, thereby ensuring high-precision torque response and superior energy efficiency even under fluctuating load conditions (Ayana et al., 2023; Levi, 1995).

To facilitate the IRFOC strategy, a Current Model flux estimator is employed to determine the rotor flux magnitude and the flux angle γ. This estimator utilizes the measured stator currents and the rotor speed as primary inputs. In this specific implementation, the estimation logic is derived directly from the third equation of the system (4), which defines the rotor flux derivative in the stationary reference frame (Ayana et al., 2023; Rivera et al., n.d.).

Unlike standard estimators, this model accounts for the presence of the iron-loss resistance R_c, which varies dynamically according to the operating frequency and flux levels. Specifically, the magnetizing current i_m^s is extracted from the stator current by compensating for the current diverted through the R_c branch. By integrating the slip frequency-calculated from the torque-producing current and the rotor time constant-with the measured mechanical speed, the instantaneous flux position γ is precisely computed. This ensures that the d-q transformation remains accurately aligned with the rotor flux linkage, even as iron losses fluctuate (Bašić & Vukadinović, 2018; Dittrich, 1998; Levi, 1995).

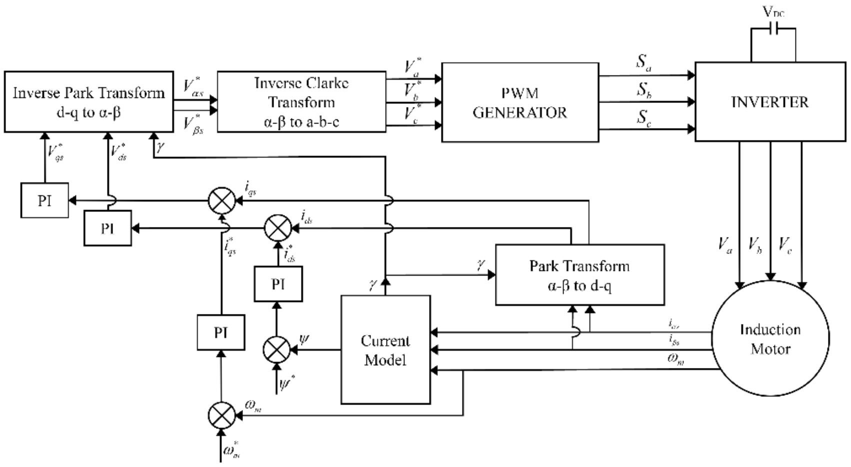

Figure 3: IRFOC System with Variable Iron-Loss Resistance Modeling

The electrical and mechanical parameters used to configure the induction motor drive model in MATLAB/Simulink are summarized in Table 1.

Table 1: Induction Motor and Drive Parameters Used in MATLAB/Simulink Simulation

Symbol	Quantity	Value	Unit
V_{DC}	DC-link Voltage	540	V
R_s	Stator Resistance	3.425	Ω
R_r	Rotor Resistance	2.786	Ω
R_c	Rated Iron-loss Resistance	1020	Ω
L_s	Stator Inductance	0.2594	H
L_r	Rotor Inductance	0.2594	H
L_m	Mutual Inductance	0.2448	H
p	Pole-pair Number	2	
J	Moment of Inertia	0.0047	kg.m^2

After configuring the simulation model using the parameter set in Table 1, two induction motor models were evaluated under the same IRFOC control structure: (i) an ideal model that neglects iron losses and (ii) an enhanced model that accounts for iron losses via the $R_c \parallel L_m$ magnetizing branch. By keeping the control structure, parameter set, and excitation conditions (speed reference, load torque, and controller gains) identical, the simulations provide a consistent basis for quantifying the impact of iron-loss modeling on speed response, electromagnetic torque, stator currents, and rotor-flux estimation accuracy.

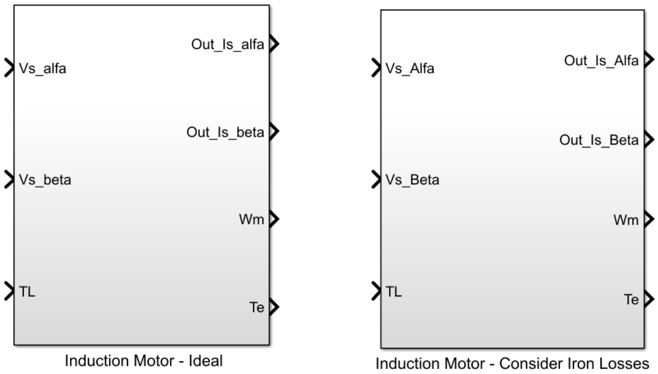

Figure 4: Induction Motor Models Used for Comparison: Ideal Model vs. Iron-Loss Model

RESULTS

In this section, the simulation results are presented to evaluate the performance of the IRFOC scheme applied to two induction motor models: an ideal model and an enhanced model that accounts for iron losses. The key variables examined include the mechanical angular speed of the rotor ω_m (reference tracking and disturbance rejection under load changes), the electromagnetic torque T_e (transient behavior and torque ripple), and the stator current i_s (current demand and its variation with operating conditions). Comparing these signals provides a consistent basis for quantifying the impact of iron-loss modeling on the drive dynamics and overall control quality across the simulated scenarios.

Table 2: Simulation test scenario: speed-reference and load-torque steps

Symbol	Quantity	From	To	Step time (s)	Unit
n_r^*	Rotor Speed Reference	0	1300	0.2	rpm
ω_m^*	Rotor Mechanical Angular Speed Reference	0	136.14	0.2	rad/s
T_L	Load Torque	0	15	2	N.m
T	Sample Time	10^{-5}			s

1. The Mechanical Angular Speed of the Rotor

The rotor mechanical angular speed ω_m, represents the rotational speed of the induction motor rotor in the mechanical domain and is a primary indicator of drive performance. In this study, ω_m is used to evaluate speed-reference tracking and disturbance rejection under identical IRFOC settings for two plant models: an ideal induction motor model and an enhanced model that accounts for iron losses. By comparing the ω_m responses of these two models under the same speed command and load conditions, the influence of iron-loss modeling on transient behavior (e.g., overshoot and settling time) and steady-state speed regulation can be quantitatively assessed.

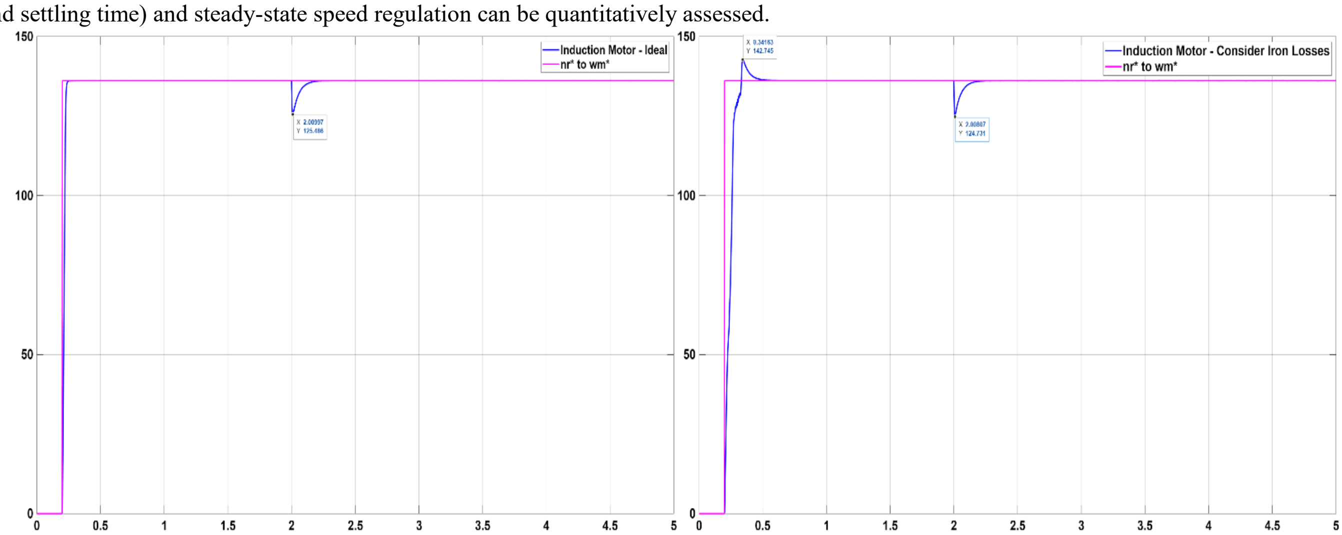

Figure 5: Mechanical Angular Speed of the Rotor showing reference tracking under IRFOC for the Ideal model and the Iron-loss model

As shown in Figure 5, both models track the speed reference following the speed step at t = 0.2s. The Ideal model reaches the reference with minimal overshoot, while the Iron-loss model exhibits a larger overshoot and more noticeable oscillations. At the load-torque step from 0 to 15 N.m applied at t = 2s, a speed dip is observed in both cases, followed by recovery, with a larger transient deviation for the Iron-loss model.

2. The Electromagnetic Torque

The electromagnetic torque T_e, represents the torque produced by the interaction between the air-gap flux and stator currents and is a primary indicator of the drive's torque-producing capability. In this study, T_e is used to evaluate the transient torque response and torque ripple under identical IRFOC settings for two plant models: an ideal induction motor model and an enhanced model that accounts for iron losses. By comparing the T_e responses of these two models under the same speed command and load conditions, the influence of iron-loss modeling on torque dynamics and load-compensation capability can be quantitatively assessed.

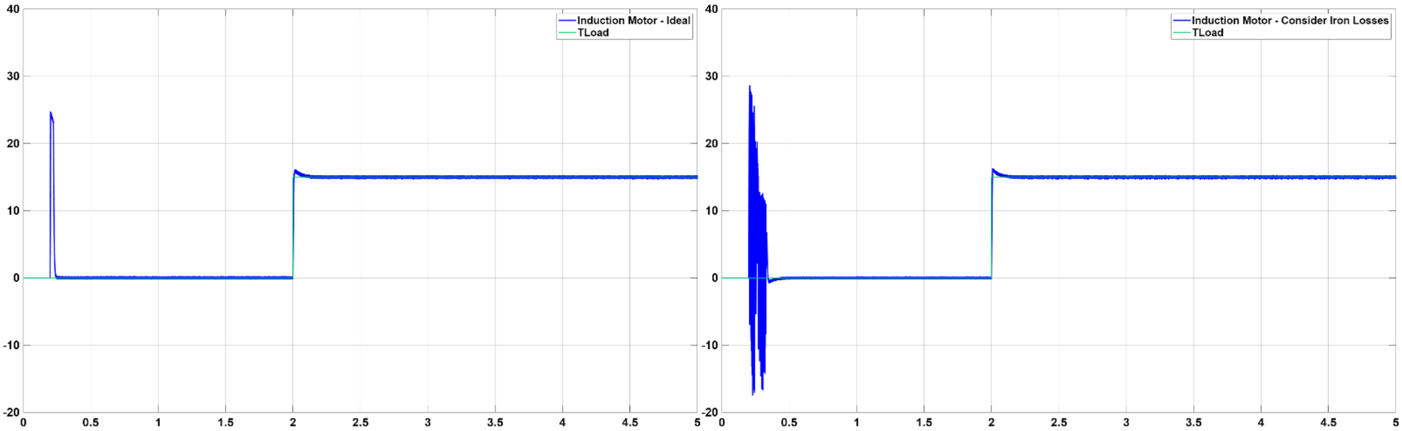

Figure 6: Electromagnetic Torque showing transient behavior and torque ripple under IRFOC for the Ideal model and the Iron-loss model

As shown in Figure 6, both models generate the required electromagnetic torque to accelerate the motor following the speed step at t = 0.2s. The Ideal model exhibits a relatively smooth torque transient with limited oscillations, whereas the Iron-loss model shows a higher initial torque fluctuation and more noticeable torque ripple during the start-up interval. At the load-torque step from 0 to 15 N.m applied at t = 2s, electromagnetic torque increases in both cases to compensate for the applied load and then settles near the commanded level, with the Iron-loss model exhibiting a larger transient deviation and higher ripple compared to the ideal model (Haddad, 2021).

3. The Stator Current

The stator current i_s, represents the current drawn by the induction motor stator and directly reflects the electrical effort required to produce the demanded flux and electromagnetic torque under IRFOC control. In this study, i_s is used to evaluate current demand and current ripple under identical IRFOC settings for two plant models: an ideal induction motor model and an enhanced model that accounts for iron losses. By comparing the i_s waveforms of these two models under the same speed command and load conditions, the influence of iron-loss modeling on the required stator current (e.g., peak and RMS values), transient behavior, and steady-state ripple can be quantitatively assessed.

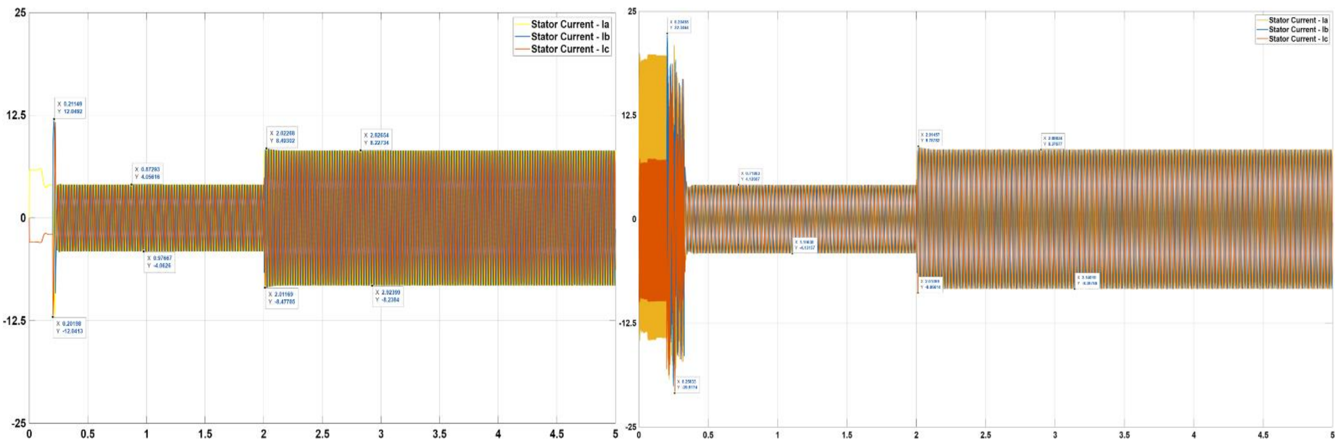

Figure 7: Stator Current showing transient behavior and torque ripple under IRFOC for the Ideal Model and the Iron-loss model

As shown in Figure 7, both models draw the required stator current to establish the commanded flux and produce the acceleration torque following the speed step at t = 0.2s. The Ideal model exhibits a smoother current transient with relatively limited oscillations, whereas the Iron-loss model shows a higher initial current fluctuation and more noticeable current ripple during the start-up interval. At the load-torque step from 0 to 15 N.m applied at t = 2s, the stator current increases in both cases to supply the additional torque demand and then settles to a higher steady-state level, with the Iron-loss model exhibiting a larger transient deviation and higher ripple compared to the Ideal model (Balamurali et al., 2020).

DISCUSSION

The simulation results confirm that the IRFOC scheme achieves stable speed regulation for both plant models, as the rotor mechanical speed converges to the reference target after the initial step and recovers following load disturbances. However, incorporating iron losses significantly alters transient characteristics. Compared to the ideal model, the model accounting for iron losses exhibits larger overshoot, more pronounced speed oscillations, and increased ripple in both electromagnetic torque and stator current. These findings suggest that neglecting iron losses leads to an overestimation of dynamic performance and an underestimation of the electrical effort required during transients and load changes.

The primary cause of this degraded transient smoothness is the additional iron-loss current component flowing through the parallel branch (modeled by iron-loss resistance). This current does not contribute to torque production; instead, it modifies the effective magnetizing current and flux dynamics perceived by the controller. Consequently, the field orientation and decoupling conditions assumed by the standard IRFOC algorithm are no longer perfectly matched to the actual plant dynamics, particularly during rapid state changes such as the speed step at t=0.2s and the load injection at t=2s. This misalignment manifests as heightened torque and current transients while the control loops compensate to maintain the desired speed.

Regarding the load-torque disturbance (0 to 15 N.m), both models increase electromagnetic torque and stator current to compensate, eventually settling at a new steady state. However, the iron-loss model demands a more aggressive transient response and exhibits greater ripple, reflecting the additional current drawn by the iron-loss branch. From a practical perspective, these results highlight the critical importance of iron-loss modeling when evaluating current demand, torque ripple, and disturbance rejection, especially under operating conditions where flux variation and frequency-dependent losses are substantial.

To ensure a rigorous comparison, identical controller gains were maintained for both models. Consequently, the increased oscillations observed in the iron-loss model could likely be mitigated by optimizing the current and speed control loops or by explicitly compensating for the iron-loss current within the flux estimator. Furthermore, this study relies on a simplified iron-loss representation and does not currently account for magnetic saturation or temperature-dependent parameter variations. Future research should address these factors to further enhance model fidelity and control accuracy.

CONCLUSION

This work evaluated an Indirect Rotor Field-Oriented Control (IRFOC) scheme applied to two induction motor models: an ideal reference model and an enhanced model explicitly accounting for iron losses via a parallel branch. Simulation results confirm that while IRFOC achieves stable speed tracking for both models under step commands and load disturbances, the iron-loss model exhibits distinct transient characteristics.

Specifically, the inclusion of iron losses results in larger transient deviations, increased speed oscillations, and higher ripple in both electromagnetic torque and stator current compared to the ideal case. These findings highlight that neglecting iron losses risks overestimating dynamic stability while underestimating the necessary current demand and torque ripple, particularly during rapid state changes. Consequently, incorporating iron-loss effects provides a much more realistic basis for assessing control quality and drive behavior.

Future research should focus on advanced controller tuning and integrating more complex loss phenomena, such as magnetic saturation and temperature-dependent parameter variations, to further enhance model fidelity and control performance (Nasir, 2020).

REFERENCES

1) Abdin, E. S., Ghoneem, G. A., Diab, H. M. M., & Deraz, S. A. (2003, November). Efficiency optimization of a vector controlled induction motor drive using an artificial neural network. In IECON'03: 29th Annual Conference of the IEEE Industrial Electronics Society (Vol. 3, pp. 2543–2548). IEEE. https://doi.org/10.1109/IECON.2003.1280646
2) Abu-Rub, H., Iqbal, A., & Guzinski, J. (2021). *High performance control of AC drives with Matlab/Simulink*. John Wiley & Sons.
3) Accetta, A., Alonge, F., Cirrincione, M., D'Ippolito, F., Pucci, M., & Sferlazza, A. (2020). GA-based off-line parameter estimation of the induction motor model including magnetic saturation and iron losses. *IEEE Open Journal of Industry Applications*, *1*, 135-147. https://doi.org/10.1109/OJIA.2020.3024567
4) Ayana, T., Wogi, L., & Morawiec, M. (2023). Core loss resistance impact on sensorless speed control of an induction motor using hybrid adaptive sliding mode observer. Archives of Electrical Engineering, 72(4). https://doi.org/10.24425/aee.2023.147417
5) Bašić, M., & Vukadinović, D. (2018). Small-size induction machine equivalent circuit including variable stray load and iron losses. Journal of Electrical Engineering & Technology, 13(4), 1604–1613. https://doi.org/10.5370/JEET.2018.13.4.1603
6) Bašić, M., Vukadinović, D., & Grgić, I. (2023). Model predictive current control of an induction motor considering iron core losses and saturation. Processes, 11, 2917. https://doi.org/10.3390/pr11102917
7) Balamurali, A., Kundu, A., Li, Z., & Kar, N. C. (2020). Improved harmonic iron loss and stator current vector determination for maximum efficiency control of PMSM in EV applications. *IEEE Transactions on Industry Applications*, *57*(1), 363-373. https://doi.org/10.1109/TIA.2020.3034888
8) Dittrich, A. (1998, September). Model-based identification of the iron loss resistance of an induction machine. In 1998 Seventh International Conference on Power Electronics and Variable Speed Drives (IEE Conf. Publ. No. 456) (pp. 500–503). IET. https://doi.org/10.1049/cp:19980577

9) Dominguez, J. R., Mora-Soto, C., Ortega-Cisneros, S., Panduro, J. J. R., & Loukianov, A. G. (2011). Copper and core loss minimization for induction motors using high-order sliding-mode control. IEEE Transactions on Industrial Electronics, 59(7), 2877–2889. https://doi.org/10.1109/TIE.2011.2171170
10) Haddad, R. Z. (2021). Iron loss analysis in axial flux permanent magnet synchronous motors with soft magnetic composite core material. *IEEE Transactions on Energy Conversion*, *37*(1), 295-303. https://doi.org/10.1109/TEC.2021.3098824
11) Karlovsky, P., Lipcak, O., & Bauer, J. (2020). Iron loss minimization strategy for predictive torque control of induction motor. *Electronics*, *9*(4), 566. https://doi.org/10.3390/electronics9040566
12) Levi, E. (1995). Impact of iron loss on behavior of vector-controlled induction machines. IEEE Transactions on Industry Applications, 31(6), 1287–1296. https://doi.org/10.1109/28.475699
13) Nasir, B. A. (2020). An accurate iron core loss model in equivalent circuit of induction machines. *Journal of Energy*, *2020*(1), 7613737. https://doi.org/10.1155/2020/7613737
14) Rivera, J., Mora-Soto, C., De La Mora, A., Di Gennaro, S., & Raygoza, J. Field Oriented Control of Induction Motors with Core Loss.
15) Tolochko, O., Kaluhin, D., & Oshurko, S. (2020). Field weakening control for induction motors based on copper and iron losses minimization. *Applied Aspects of Information Technology*, *3*(2), 44-57. https://doi.org/10.15276/aait.02.2020.3
16) Tran, C. D., Kuchar, M., & Nguyen, P. D. (2024). Research for an enhanced fault-tolerant solution against the current sensor fault types in induction motor drives. *Electrical Engineering & Electromechanics*, (6), 27-32. https://doi.org/10.20998/2074-272X.2024.6.04
17) Tran, C. D., Kuchar, M., & Nguyen, P. D. (2025). Improved speed sensorless control for induction motor drives using rotor flux angle estimation. *Electrical Engineering & Electromechanics*, (6), 93-97. https://doi.org/10.20998/2074-272X.2025.6.12
18) Tran, C. D., Kuchar, M., Sotola, V., & Nguyen, P. D. (2025). Sensor fault diagnosis strategy based on rotor flux observers in three-phase induction motor drive. *Scientific Reports*. https://doi.org/10.1038/s41598-025-29381-9

Corresponding Author: Thinh Ba Cong Huynh